atmosphere

MDPI

Article

A Comprehensive Flash Flood Risk Assessment Framework for Mountainous Regions: A Case Study in Chongqing, China

Jing Qin [1,*], Lu Wang [1,*], Lingyun Zhao [1], Jie Niu [2], Mingming Zhu [1], Yaning Yi [1], Ruihu Yao [1] and Wenlong Niu [1]

[1] China Institute of Water Resources and Hydropower Research, Beijing 100038, China; zhaolingyun1@iwhr.com (L.Z.); zhumingming@iwhr.com (M.Z.); yiyn@iwhr.com (Y.Y.); yaorh@iwhr.com (R.Y.); niuwl@iwhr.com (W.N.)

[2] Jinan Water Conservancy Building Survey, Design and Research Institute Co., Ltd., Jinan 250100, China; niujie1117@163.com

* Correspondence: qinjing@iwhr.com (J.Q.); wlbless@iwhr.com (L.W.); Tel.: +86-10-68785589 (L.W.)

Abstract

Quantitative risk assessment of flash floods is crucial for developing disaster prevention and mitigation strategies. This study developed a refined framework that innovatively integrates field-validated data from Chongqing's flash flood disaster investigation project with AHP, factor analysis, and cluster analysis to quantify hazard, vulnerability, resistance, and risk indicators at a 30 m grid. Unlike existing coarse-scale assessments that rely on generic indicators, this hybrid model, calibrated by observed disaster evidence, significantly enhanced the local relevance and reliability of risk zoning. The validity of this framework was confirmed through validation against objective weighting methods and historical flash flood locations. The results indicated that the risk value of flash floods in Chongqing was between 0.24 and 0.69, with extremely high-risk and high-risk zones covering 42,388 km^2 (51.47%) of the study area. This accurately identifies areas at high risk of flash floods and provides a basis for government decision-making regarding priority areas for disaster risk reduction investments. Verification showed that 83.44% of historical disaster points fall within medium-risk or above zones, confirming the framework's accuracy in identifying flood-prone hotspots and providing actionable support for targeted early warning and resource allocation.

Keywords: flash flood; risk assessment; survey and evaluation data; Chongqing; China

1. Introduction

Flash floods are rapidly accumulating floods that occur in small mountainous basins. As a common natural disaster in China, flash floods are characterised by suddenness, high frequency, and poor predictability [1]. The flash flood prevention and control area in China covers an area of 3.86 million square kilometres, threatening 570,000 villages and 300 million people. Since the 1990s, China's flash floods have accounted for more than 60% of flood disasters and have been the main factor raising the severity of flood disasters [2]. Chongqing is located in the transitional zone between the Tibetan Plateau and the middle and lower reaches of the Yangtze River, where mountainous and hilly terrain covers more than 90% of the territory [3]. Complex topographic and geological conditions, frequent rainstorms, dense population distribution, and excessive human activities have led to frequent flash floods in Chongqing. From 2001 to 2019, 364 rainstorms and floods occurred in Chongqing, causing economic losses of 53.745 billion yuan, and 763 people were killed or missing, of which more than 70% were caused by flash floods alone [4]. In

Check for updates

Academic Editor: Tin Lukić

Received: 18 March 2026
Revised: 19 May 2026
Accepted: 19 May 2026
Published: 21 May 2026

Copyright: © 2026 by the authors. Licensee MDPI, Basel, Switzerland. This article is an open access article distributed under the terms and conditions of the Creative Commons Attribution (CC BY) license.

the context of climate change, the frequency and intensity of heavy precipitation in some regions are projected to increase [5,6]. Chongqing is likely to encounter more frequent flash floods, which will adversely affect the defence work implemented by government departments and the public. Therefore, conducting scientific flash flood risk assessments is of considerable significance for understanding the distribution of flash flood risk areas in Chongqing.

Many studies have recently been conducted on the risk assessment of natural disasters [7–13], with scholars generally focusing on the flood risk of major rivers and urban waterlogging risk, drought risks, and flash flood risks [14–18]. The AHP is simple to calculate and suitable for multi-objective decision analysis, and it is widely used in risk assessment. For example, a multi-criteria analytical model based on the AHP-entropy method was used for long- and short-term flood risk evaluation of the Poyang Lake Basin, which considered six flood hazard factors and four flood vulnerability factors, namely maximum three-day rainfall and population density [19]. A methodology for comprehensively assessing flash flood risk was used in Guangdong Province, China, using the improved AHP and the maximum likelihood clustering algorithm [11]. Many influencing factors were incorporated into the assessment model, such as rainfall [20], underlay, slope, vegetation cover, and economic properties, all of which contributed to the regional flash flood defence capability [21,22]. These studies provided valuable knowledge, yet they exhibited two main limitations when applied to flash flood risk in mountainous regions. First, the assessments were typically conducted at coarse spatial scales and thus could not effectively identify the small river channels where flash floods actually originated. Second, the indicator systems relied heavily on generic, readily available geospatial data (e.g., regional rainfall, topography, and population density) [21,23], while the findings of dedicated flash flood disaster investigation and evaluation projects, which contained rich field-validated information [24] (e.g., historically calibrated rainfall thresholds, surveyed at-risk populations, existing monitoring stations, and flood control capacities), remained largely unused. Ignoring these empirically grounded data might result in inaccurate identification of risk factors and an inability to reflect local disaster prevention capabilities.

To address these gaps, this study developed a refined flash flood risk assessment framework for mountainous regions. The primary novelty lay not in the use of AHP and GIS tools themselves, but in how we grounded the framework with high-resolution, field-validated data and implemented the assessment at a fine spatial resolution. In doing so, we shifted the AHP framework from a purely expert-driven model to a hybrid model calibrated by field-validated data, thereby significantly enhancing the reliability and local relevance of risk zoning. Furthermore, the synergistic combination of enriched indicators and refined assessment units yielded a risk map with markedly improved spatial accuracy, which more precisely delineated high-risk hotspots and effectively reduced both overgeneralisation and false positives, offering a more trustworthy basis for targeted early warning and mitigation resource allocation.

Specifically, the study established a flash flood disaster risk assessment framework based on risk assessment theory by AHP [25], factor analysis, and cluster analysis [26], with Chongqing, China, as the study area and an assessment unit of 30 m. In particular, we innovatively integrate the achievements of Chongqing's flash flood disaster investigation and evaluation project into the AHP indicator system. The indicators considered in this study include meteorological conditions (composite rainfall indicator and threshold rainfall), underlay conditions (slope, NDVI, and river network density), population indicators (population density in flash flood control areas), economic property indicators (proportion of primary industry output), monitoring capacity indicators (density of automatic monitoring stations), and flood protection capacity indicators (current flood protection

capacity). Data marked with an underscore are derived from the results of surveys and evaluations conducted in the last decade. These datasets are intrinsically linked to the region's actual risk characteristics and are transformed into quantitative, spatially explicit indicators. Based on this risk assessment framework, the risk of flash flood disasters was quantified systematically and scientifically. This study demonstrates the following: (i) distribution of flash flood hazard, vulnerability, and resistance in Chongqing and its districts; (ii) distribution of flash flood risk in Chongqing and its districts; and (iii) area and distribution of risk zones with four levels of risk: low, medium, high, and extremely high in Chongqing and its districts. Section 2 describes the study area and its data. Section 3 describes the risk assessment framework used in this study. Section 4 presents the results and analysis. Section 5 discusses the accuracy of the research results. Finally, the conclusions are presented in Section 6.

2. Study Area and Data

2.1. Study Area

Chongqing is located in southwest China and is bordered by Hubei and Hunan in the east, Guizhou in the south, Sichuan in the west, and Shaanxi in the north. Chongqing is 470 km long from east to west and 450 km wide from north to south, covering an area of 82,400 km^2, with jurisdiction over 38 districts, counties, and 1031 townships.

Chongqing has a highly undulating topography, with higher elevations in the east, south, and southeast, and lower elevations in the west (Figure 1). The region features diverse landforms, which are primarily classified into eight categories: medium-low mountains, low mountains, high hills, medium hills, low hills, gentle hills, plateaus, and plains. Mountains and hills account for more than 90% of the city's total area [3,27]. The river system in the territory is dense and developed, forming a river network with the Yangtze River as the main trunk, the Jialing River and Wujiang River as branches, and secondary tributaries distributed in the form of branches. Chongqing is located in the subtropical warm and humid monsoon climate zone, with hot summer and warm winter, light and heat in the same season, distinct rainy seasons, heavy rainfall intensity, an annual average temperature of 18–19 °C, and annual precipitation days of 120–170 days.

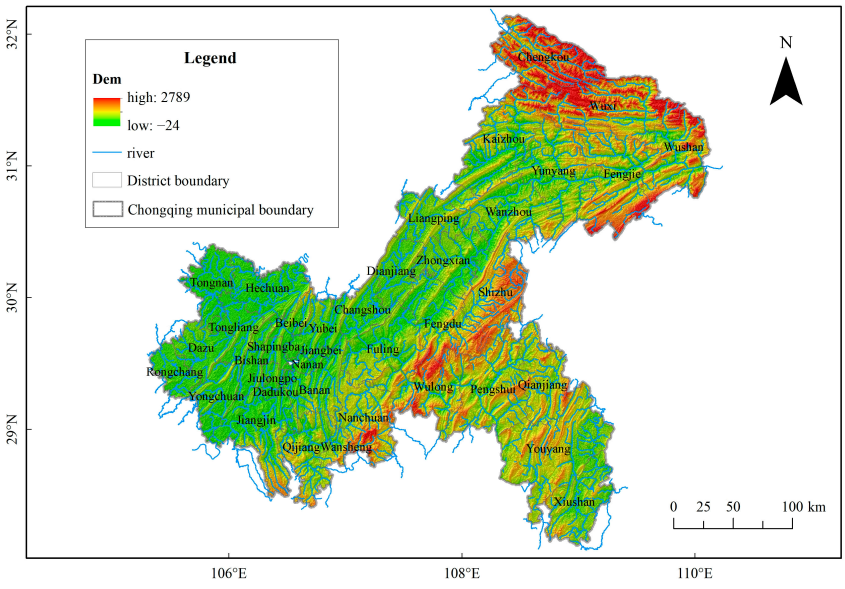


Figure 1. Zoning diagram of Chongqing.

2.2. Research Data

The information related to the data used in this study was presented in Table 1. The data used in this analysis and calculation of flash flood risks was obtained from Chongqing's flash flood disaster investigation and evaluation report and the dynamic update report for dangerous zones, covering the period from 2013 to 2023. Chongqing's updated list of 4020 dangerous zones provides information on design rainfall, rainfall thresholds for warnings, and current protective capabilities. The DEM and NDVI data are disclosed by the geospatial data cloud (https://www.gscloud.cn/ (accessed on 30 May 2023)). Proportion of output value of primary industry was sourced from the Chongqing Statistical Yearbook. The spatial scale for this assessment was 30 m, and data with inconsistent spatial scales were resampled. For point data, the inverse distance weighting interpolation method is used to convert it into raster data with a spatial resolution of 30 m.

Table 1. Data sources.

Data	Sources	Description
Design rainstorm	Design heavy rain in dangerous areas	4020 points
Threshold rainfall	Critical rainfall in danger areas	4020 points
DEM	Geospatial data cloud	30 m spatial resolution
NDVI	Geospatial data cloud	0.0059 degree spatial resolution
River system	Flash flood disaster prevention project work base map	/
Population in the danger zone	Population and area of the control zone	38 districts
Proportion of output value of primary industry	Chongqing Statistical Yearbook 2021	/
Monitoring station	Chongqing Water Resources Bureau	1105 monitoring stations

3. Risk Assessment Framework for Flash Flood Based on Risk Assessment Theory

3.1. Risk Assessment Theory

According to the theory of natural disaster risk [9], the risk of natural disasters consists of three aspects: the hazardousness of disaster-causing factors, the vulnerability of disaster-prone entities, and the capacity for disaster prevention and mitigation [28]. Hazard and vulnerability are positive indicators, while resilience is a negative indicator. However, no unified model currently exists describing the specific mechanisms of action. Addition and multiplication models are typically used for this purpose. In this study, we adopted a three-factor summation model for assessing the risk of flash floods. The assessment model was as follows:

$$F = we \times E + wv \times V + wp \times (1 - R) \quad (1)$$

where F represents the risk of flash floods; E represents the hazard risk index of the causative factor; V represents the vulnerability index of the exposed body; R represents the disaster prevention and reduction capacity index; and we, wv, and wp represent the weights of the indices.

3.2. Indicators for the Risk Assessment of Flash Flood

To construct a hierarchical structure with clear logical relationships and accurate indicator meanings for the evaluation model, this study collected relevant materials on flood control and disaster prevention construction and consulted experts in the field of flood control. The target decomposition principle and AHP were applied to systematically organise, analyse, and prioritise flash flood risk indicators in Chongqing.

The flash flood risk assessment was based on data analysis results and expert opinions and comprised hazard, vulnerability, and disaster resistance (Figure 2). For composite indicators, this study employed factor analysis (FA) to reduce their dimensionality. To avoid overlap or feedback relationships among the indicators, this study examined the independence of similar indicators using Pearson's correlation coefficient. The results showed that the correlation coefficients between the indicators were low, suggesting that they are independent of one another. Additionally, we have incorporated the impact of these indicators on flash flood risk to characterize their interaction (Table 2).

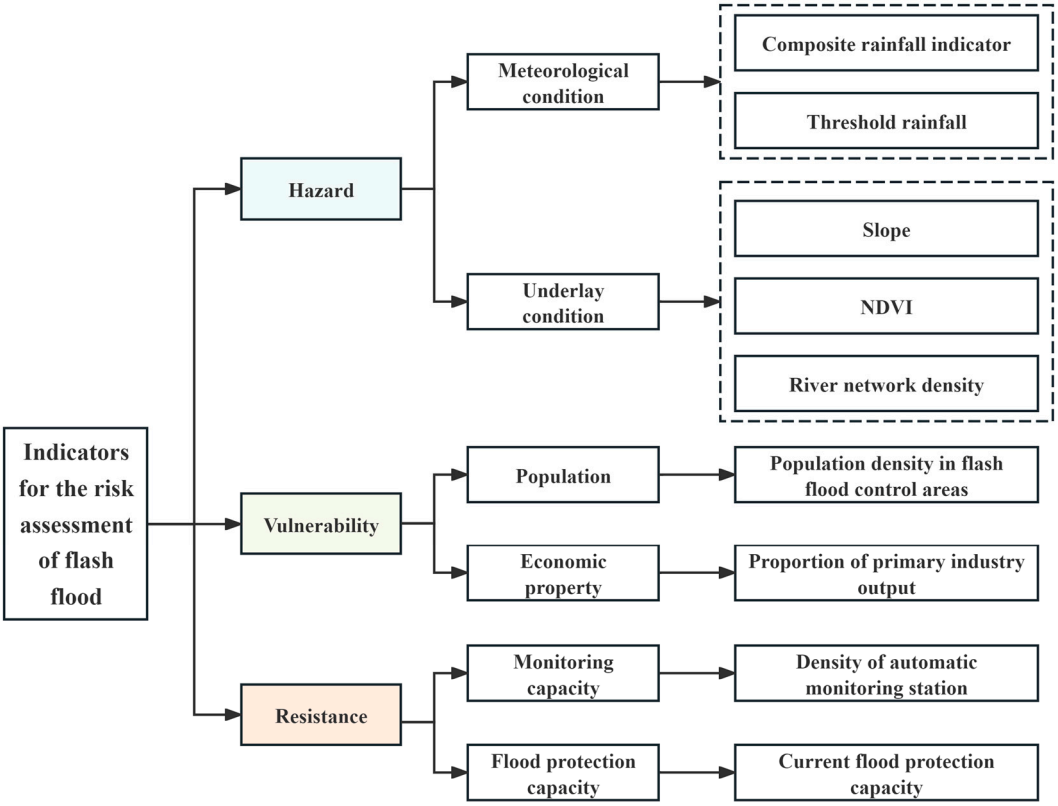


Figure 2. Indicators used in this study.

Table 2. Evaluation indicators and their impact on risk.

Primary Indicators	Secondary Indicators	Tertiary Indicators	Risk Characteristics (Positive or Negative)
Hazard (*E*)	Meteorological condition (MC1)	Composite rainfall indicator (CE1)	+
		Threshold rainfall (CE2)	−
	Underlay condition (UC)	Slope (CE3)	+
		NDVI (CE4)	−
		River network density (CE5)	+
Vulnerability (V)	Population (P)	Population density in flash flood control areas (CV1)	+
	Economic property (EP)	Proportion of primary industry output (CV2)	+
Resistance (*R*)	Monitoring capacity (MC2)	Density of automatic monitoring stations (CR1)	+
	Flood protection capacity (FP)	Current flood protection capacity (CR2)	−

3.2.1. Hazard Indicators

1. Meteorological conditions
    - Composite rainfall indicator
      Five design storms with return periods of 5, 10, 20, 50, and 100 years and four standard calendars of 10 min, 1 h, 6 h, and 24 h were downscaled by FA to obtain a composite indicator of the storm elements.
    - Threshold rainfall
      Threshold rainfall is the core parameter of the rainfall warning method and represents the magnitude and intensity of the field rainfall that is reached or exceeded when flash flooding occurs in a watershed or region. It is derived by comprehensively considering the rainfall intensity, field cumulative rainfall, previous rainfall, and other factors. This indicator was calculated by taking the arithmetic mean of the 1 h and 3 h critical rainfall amounts.
2. Underlay conditions
    - Slope
      The slope is an extremely important indicator of risk assessment for flash floods because it effectively reflects the steepness of the surface. In the event of flash floods, areas with greater slopes have a shorter convergence time, leading to a reduction in the time required to form flood peaks, which further increases the threat posed by flash floods. This study used the DEM of the study area to extract the slope.
    - River network density
      River network density can well characterise the scouring effect of the river using the ratio of the total length of the mainstream in the watershed to the area of the watershed.
    - NDVI
      Vegetation mitigates the direct scouring of slope soils through surface runoff, thereby preventing and slowing the occurrence of flash floods.

3.2.2. Vulnerability Indicators

1. Population indicators

Population density in the flash flood control area is the number of people per unit of land area in the flash flood control area, which reflects the distribution of the number of people in the control area.

2. Economic property indicators

The proportion of primary industry output in GDP represents the proportion of GDP accounted for by industries such as agriculture that derive their products directly from nature, and it reflects the distribution of economic activity within a specific region.

3.2.3. Resistance Indicators

1. Density of automatic monitoring stations

The density of automatic monitoring stations is calculated by dividing the area of the jurisdiction by the number of stations, reflecting the region's capacity to monitor rainfall and water conditions.

2. Current flood protection capacity

Current flood control capacity reflects the level of flash flood prevention and mitigation in each hazardous area.

3.2.4. Dimension Reduction for Composite Indicators

FA is a multivariate statistical analysis method that starts from the internal dependency relationship of the correlation matrix of research indicators, and reduces the number of variables with overlapping information or complex interrelationships to a few uncorrelated comprehensive factors. In FA, the common factors are unobservable but objectively existing common influencing factors. Each variable can be expressed as the sum of a linear function of the common factors and a specific factor:

$$X_i = a_{i1}F_1 + a_{i2}F_2 + \ldots + a_{im}F_m + \varepsilon_i \ (i = 1, 2, 3 \ldots, p) \quad (2)$$

where $F_1, F_2, \ldots, F_m$ represents the common factor, and ε_i is the specific factor of X_i. This model can be expressed in matrix form as:

$$X = AF + \varepsilon \quad (3)$$

$$X = \begin{bmatrix} X_1 \\ X_2 \\ \cdots \\ X_p \end{bmatrix}, \ P = \begin{bmatrix} a_{11} & a_{12} & \cdots & a_{1m} \\ a_{21} & a_{22} & \cdots & a_{2m} \\ \cdots & \cdots & \cdots & \cdots \\ a_{p1} & a_{p2} & \cdots & a_{pm} \end{bmatrix}, F = \begin{bmatrix} F_1 \\ F_2 \\ \vdots \\ F_m \end{bmatrix}, \varepsilon = \begin{bmatrix} \varepsilon_1 \\ \varepsilon_2 \\ \vdots \\ \varepsilon_p \end{bmatrix} \quad (4)$$

Before applying FA, it is necessary to conduct a feasibility test on the original data. The KMO test and Bartlett's test are used to determine whether there is a correlation among the original data.

For the KMO value, a value of 0.9 or above is highly suitable for conducting factor analysis, a value between 0.7 and 0.9 is appropriate, a value between 0.6 and 0.7 is acceptable, a value between 0.5 and 0.6 indicates poor suitability, and a value below 0.5 should be abandoned.

For Bartlett's test, if $P < 0.05$, the null hypothesis is rejected, which means factor analysis can be conducted. If the null hypothesis is not rejected, it indicates that these variables may independently provide some information and are not suitable for factor analysis.

3.3. Determination of Assessment Indicator Weights

Determining the weight of each indicator is an important task and a key link in establishing an assessment indicator system [29,30]. To make the method of determining the weights of indicators both scientifically sound and operationally simple, this study employed a simplified Delphi method combined with the hierarchical analysis method; that is, the initial fuzzy weights were first determined by the single-round expert consultation method, and then AHP was used to process and test the initial weights. Finally, the quantitative weights of each indicator were derived.

3.3.1. Quantitative Scales for Determining the Importance of Indicators

To measure the importance of the assessment indicators, an expert questionnaire was designed to solicit 12 experts who had been engaged in flash flood prevention and control for many years to compare the ratio of the importance of the indicators at the same level and T.L. Satty's 1–9 ratio scale method was employed (Table 3).

Table 3. T.L. Satty's 1–9 ratio scaling method.

Scale	Significance
1	αi is as important as αj
3	αi is slightly more important than αj
1/3	αi is slightly less important than αj

Table 3. *Cont.*

Scale	Significance
5	αi is significantly more important than αj
1/5	αi is significantly less important than αj
7	αi is much more important than αj
1/7	αi is much less important than αj
9	αi is absolutely more important than αj
1/9	αi is absolutely unimportant compared to αj
2, 4, 6, 8	median of two neighbouring judgments
1/2, 1/4, 1/6, 1/8	median of two neighbouring judgments

Note: αi and αj are two evaluation indicators of the same level. Judgement relative to some evaluation index at the upper level. A compromise between these two judgments is required.

3.3.2. Constructing Judgement Matrices

A judgement matrix is a representation of the ratios provided by experts regarding the relative importance of each factor at each level. The judgement matrix is the foundation of the hierarchical analysis method, and constructing this matrix is a crucial step of the method [31]. After the calculation, the judgement matrix established in this case was as follows (Tables 4–7).

Table 4. Judgement matrix for primary indicators.

Indicators	E	V	R
E	1	2	3
V	1/2	1	2
R	1/3	1/2	1

Table 5. Judgement matrix for tertiary indicators (hazard indicators).

Hazard	CE1	CE2	CE3	CE4	CE5
CE1	1	1/2	2	3	3
CE2	2	1	3	3	3
CE3	1/2	1/3	1	2	2
CE4	1/3	1/3	1/2	1	1
CE5	1/3	1/3	1/2	1	1

Table 6. Judgement matrix for tertiary indicators (vulnerability indicators).

Vulnerability	CV1	CV2
CV1	1	3
CV2	1/3	1

Table 7. Judgement matrix for tertiary indicators (resistance indicators).

Resistance	CR1	CR2
CR1	1	1
CR2	1	1

3.3.3. Determination of Indicator Weights

The main methods for calculating indicator weights in AHP [32] are the power, square root, and sum-product methods. To simplify the calculation, we processed and calculated the 12 expert scoring sheets collected, determined the degree of importance of each indicator,

and used the square root method to calculate and obtain the weights of the indicators (Table 8).

Table 8. Indicator weights at various levels.

Primary Indicators	Weights	Secondary Indicators	Weights	Tertiary Indicators	Weights
E	0.54	MC1	0.65	CE1	0.41
				CE2	0.59
		UC	0.35	CE3	0.45
				CE4	0.27
				CE5	0.27
V	0.3	P	0.75	CV1	1
		EP	0.25	CV2	1
R	0.16	MC2	0.5	CR1	1
		FP	0.5	CR2	1

3.4. Calculation of Flash Flood Risk

The indicators were first normalised using the ArcGIS 10.8 fuzzy affiliation tool to convert the input raster to a range of zero to one. Based on the risk assessment model and the hazard, vulnerability, and resistance indicators, the weights of the indicators were determined according to the equations in Section 3.1, and the weights of the indicators are determined in Section 3.3.3. A raster weighting calculation using ArcGIS 10.8 was used to obtain the degree of the flash flood risk.

3.5. Division of Flash Flood Risk Zones

Considering the geographic and socioeconomic zoning and other factors, according to the distribution of the degree of risk of flash flood disasters, the Iso clustering unsupervised classification tool in ArcGIS was used to classify the risk of flash flood disasters. The risk was divided into four levels, corresponding to low-, medium-, high-, and very high-risk zones.

4. Results and Analysis

4.1. Analysis of Flash Flood Hazard Indicators

4.1.1. Analysis of Hazard Secondary Indicators

1. Meteorological condition

Based on the investigation and evaluation report of flash flood disasters in all districts and counties of the Chongqing Municipality, the results of the design storm calculation for each danger zone were collected and organised. After data verification, the number of valid danger zones was 4020. The calculation of the indicators is described in Section 3.2.

The KMO test value was between 0.7 and 0.9, and the *p*-value in Bartlett's test passed the test at the 1% significance level, allowing for factor analysis (Table 9). A scree plot was generated to show the relationship between the number of factors and the eigenvalues. The slope of the plot flattens out when five factors are used (Figure 3). Additionally, the factor weight analysis indicates that five factors produce a cumulative variance explained of over 92% after rotation (Table 10), which exceeds the commonly adopted threshold of 85%. Therefore, five factors were retained in this study. The component matrix table (Table 11) shows the factor score coefficients (principal component loadings) included in each component, which were used to calculate component scores. Factors 1 and 2 were found to primarily represent the 24 h and 6 h design rainstorm amounts for the five

frequency intervals, while Factors 3, 4, and 5 primarily represented the 10 min and 1 h design rainstorm amounts for the same intervals.

Table 9. KMO and Bartlett tests.

KMO		0.719
Bartlett Sphericity Test	Approximate chi-square	258,272.344
	df	190.000
	P	0.000 ***

Note: *** indicates significance at the 1% level.

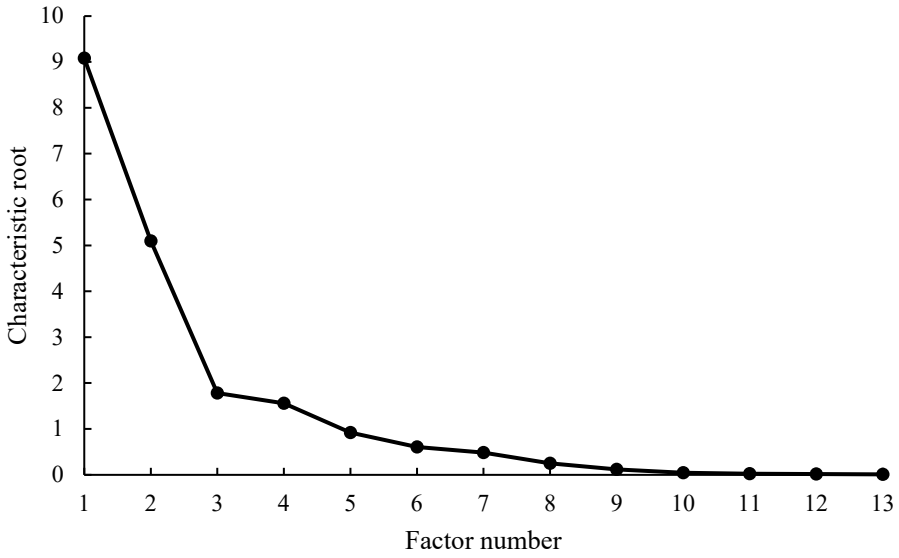


Figure 3. Factor analysis gravel chart.

Table 10. Factor weighting results.

Index	Explanatory Rate of Variance After Rotation (%)	Cumulative Variance Explained After Rotation (%)	Weights (%)
Factor 1	24.162	24.162	26.216
Factor 2	22.638	46.8	24.562
Factor 3	21.464	68.264	23.289
Factor 4	18.581	86.845	20.161
Factor 5	5.321	92.166	5.773

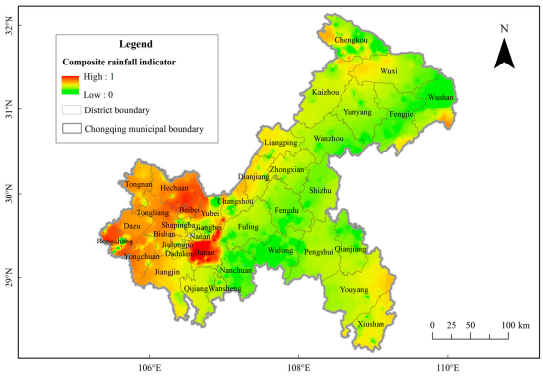
Table 11. Ingredient matrix for FA.

Index	Components				
	Component 1	Component 2	Component 3	Component 4	Component 5
1% 10min YL	0.016	0.053	0.458	0.134	0.213
1% 1h YL	0.008	0.059	0.489	0.131	−0.064
1% 6h YL	0.024	0.171	0.206	0.002	0.11
1% 24h YL	0.102	0.039	0.051	0.067	0.122
2% 10min YL	0.016	0.055	0.459	0.144	0.202
2% 1h YL	0.009	0.066	0.485	0.114	−0.144
2% 6h YL	0.017	0.173	0.156	0.207	0.056
2% 24h YL	0.104	0.031	0.069	−0.136	0.098
5% 10min YL	−0.014	0.028	0.087	0.611	0.083
5% 1h YL	−0.005	0.059	0.171	0.514	−0.103
5% 6h YL	0.019	0.174	0.153	0.203	0.006
5% 24h YL	0.105	0.03	0.056	−0.138	0.078

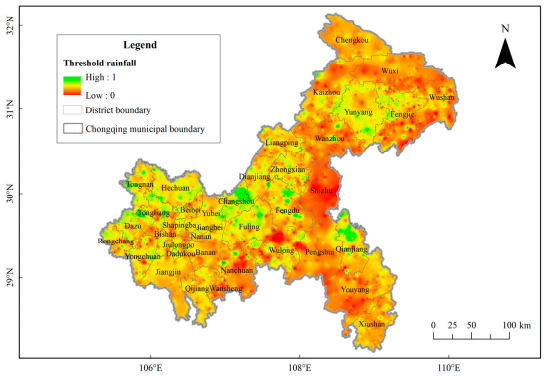
Table 11. *Cont.*

Index	Components				
	Component 1	**Component 2**	**Component 3**	**Component 4**	**Component 5**
10% 10min YL	−0.014	0.021	0.088	0.586	0.18
10% 1h YL	−0.013	0.044	0.238	0.525	−0.129
10% 6h YL	0.021	0.173	0.15	0.205	−0.032
10% 24h YL	0.105	0.028	0.042	−0.136	0.056
20% 10min YL	0.025	0.005	0.011	0.036	1.01
20% 1h YL	−0.001	0.034	0.444	0.12	−0.078
20% 6h YL	0.031	0.167	0.187	0.002	−0.05
20% 24h YL	0.104	0.033	−0.005	0.058	0.042
20% 24h YL	0.104	0.033	−0.005	0.058	0.042

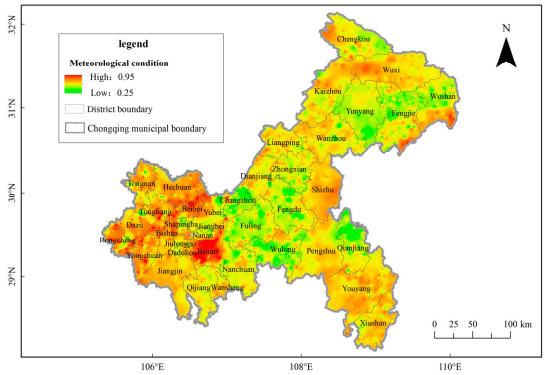
The factors under each principal component were obtained by multiplying the component matrix table with the design storm values at the five design frequencies and the four standard calendar times, and the factors under each principal component were obtained using the formula F = (0.242/0.922) × F1 + (0.226/0.922) × F2 + (0.215/0.922) × F3 + (0.186/0.922) × F4 + (0.053/0.922) × F5 to obtain the composite rainfall indicator (Figure 4a). The threshold rainfall was also calculated as described in Section 3.2.1 (Figure 4b).



(**a**) Composite rainfall indicator.



(**b**) Threshold rainfall.



(**c**) Meteorological condition indicators.

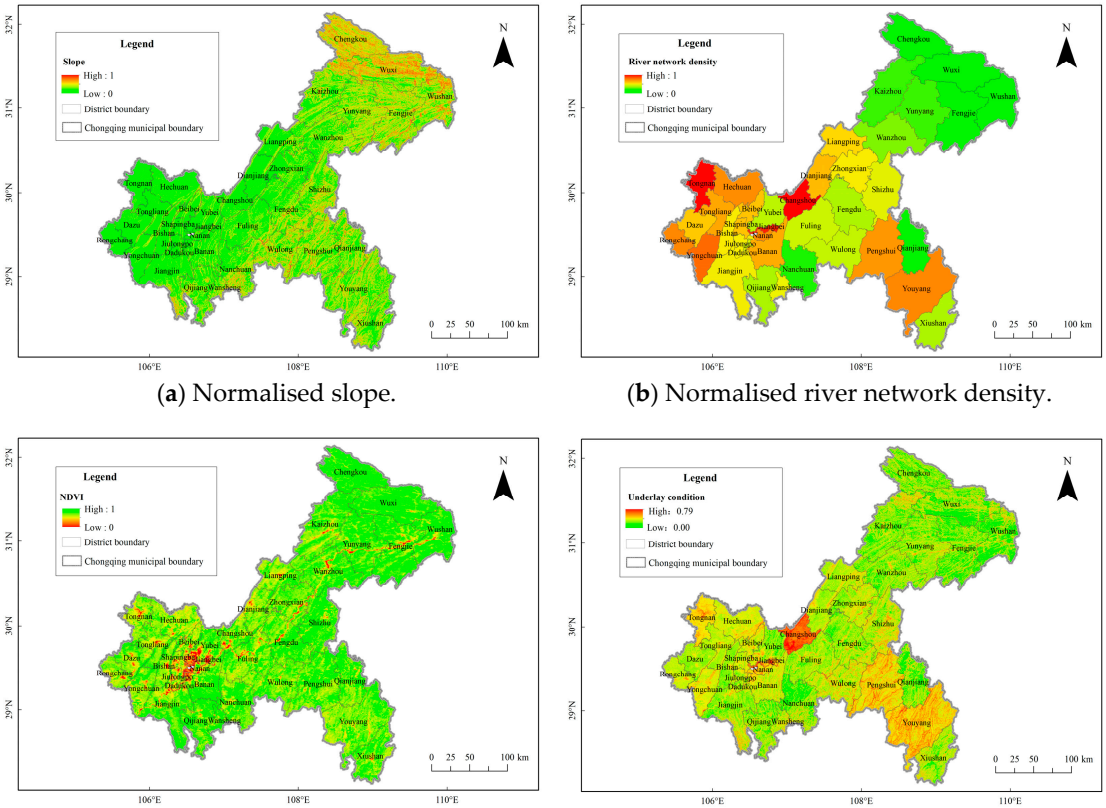
Figure 4. Normalised composite rainfall (**a**), normalised threshold rainfall (**b**), and meteorological condition indicators (**c**) for Chongqing municipality.

Meteorological conditions were calculated using the weights of the components of the secondary hazard indicators identified in Section 3.3.3 (Figure 4c). Meteorological conditions showed that the indicator value was large and the danger was high in Banan, Beibei, Hechuan, Tongliang, Dazu, Rongchang, Yongchuan, and other districts in the main city metropolitan area, Wuxi, Wushan, Kaizhou, and other districts in the northeastern region of

Chongqing, and Youyang, Shizhu, Xiushan, and other districts in the southeastern region of Chongqing. The high precipitation risk was primarily because these areas had higher design rainfall levels, yet the critical rainfall threshold for flash floods was relatively low.

2. Underlay condition

As outlined in Section 3.2.1, the slope, NDVI, and river network density indicators were also calculated (Figure 5a–c). The underlay condition was then calculated using the weights of the components of the secondary hazard indicators identified in Section 3.3.3 (Figure 5d). The underlay conditions showed that the indicators were larger and more dangerous in districts such as Changshou, Jiangbei, and Nan'an in the main urban metropolitan area and Pengshui and Youyang in southeastern Chongqing. The high risk associated with these land surface conditions was due to potential factors including steeper slopes, well-developed river systems, and low vegetation coverage, which together resulted in a higher risk of flash floods.



(**a**) Normalised slope. (**b**) Normalised river network density.

(**c**) NDVI. (**d**) Underlay condition indicators.

Figure 5. Normalised slope (**a**), normalised river network density (**b**), NDVI (**c**), and underlay condition indicators (**d**) for Chongqing municipality.

4.1.2. Analysis of Hazard Primary Indicators

The hazard indicators were the result of a combination of meteorological and underlying conditions (Figure 6). Banan, Beibei, Hechuan, Tongnan, Rongchang, Yongchuan, and other districts in the main city metropolitan districts; Wuxi, Kaizhou, and other districts in northeastern Chongqing; and Shizhu, Youyang, Xiushan, Pengshui, and other districts in southeastern Chongqing had high hazard indicator values.

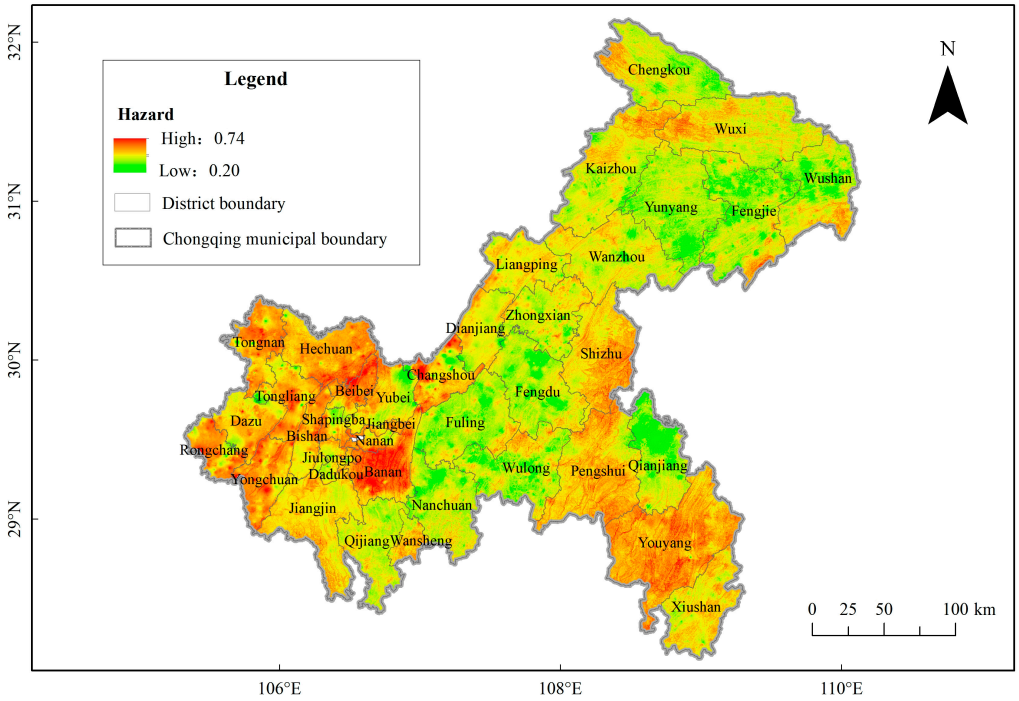


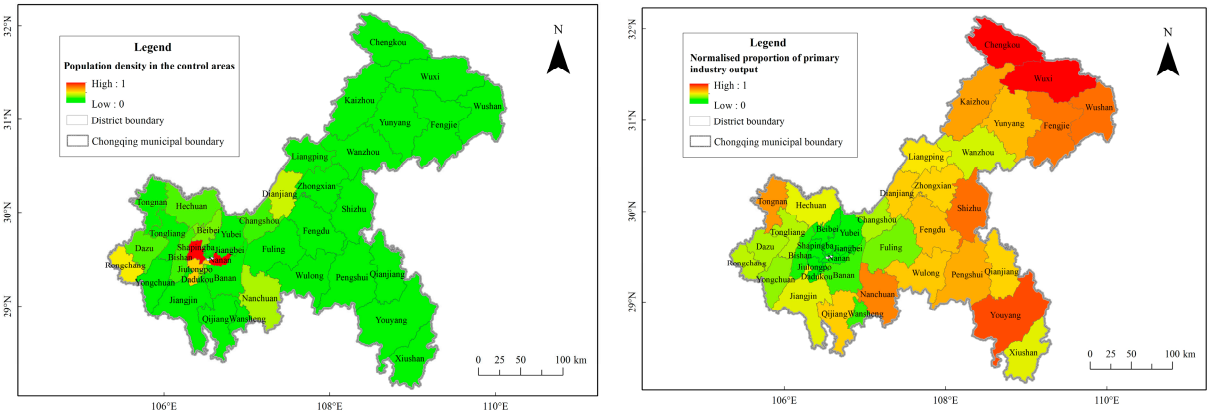
Figure 6. Distribution of hazard indicators in Chongqing.

4.2. Analysis of Flash Flood Disaster Vulnerability

4.2.1. Analysis of Secondary Index of Vulnerability

1. Population

As described in Section 3.2.2, the population density in the control areas was also calculated (Figure 7a). Population density in the control areas reflected the distribution of population indicators, showing that districts and counties such as Nan'an and Shapingba had higher population densities in their control areas, while those in the northeastern and southeastern parts of Chongqing had lower population densities. This distribution was due to the fact that the control areas in districts and counties such as Nan'an and Shapingba were relatively small, located within the main urban area, and had a relatively concentrated population distribution, which in turn resulted in higher population densities in these control areas.



(**a**) Normalised population density in the control areas. (**b**) Normalised proportion of primary industry output.

Figure 7. Normalised population density in the control areas (**a**) and proportion of primary industry output (**b**) for Chongqing municipality.

2. Economic property

As outlined in Section 3.2.2, the proportion of primary industry output was calculated as a representation of economic property indicators (Figure 7b). The distribution map showed that the share of primary industry output was higher in northeastern and southeastern Chongqing and lower in the central and western regions, which is consistent with the economic development patterns of the city's various districts. This distribution arose because the northeastern and southeastern regions were primary agricultural production areas and ecological conservation zones, where the primary industry was the main focus of development.

4.2.2. Analysis of Vulnerability Primary Indicators

According to the calculation results in the previous sections, among the secondary vulnerability indices, the population index was higher than the economic property index, and the specific weight values are listed in Table 8.

The risk distribution map of the vulnerability index (Figure 8) showed that the vulnerability risk of Nan'an, Shapingba, Rongchang, and other districts in the main metropolitan area was higher, whereas the vulnerability risk in northeast and southeast Chongqing was lower. This is because the population index accounts for 75% of the secondary vulnerability indices. The control area of the main urban area has a large population density, a high urbanisation rate, and a developed social economy, resulting in an increased flash flood disaster vulnerability. The population density of southeast and northeast Chongqing and the population density of the prevention and control areas are relatively small, the proportion of output value of the primary industry is high, and the level of economic development is relatively low; therefore, the vulnerability to flash flood disasters is low.

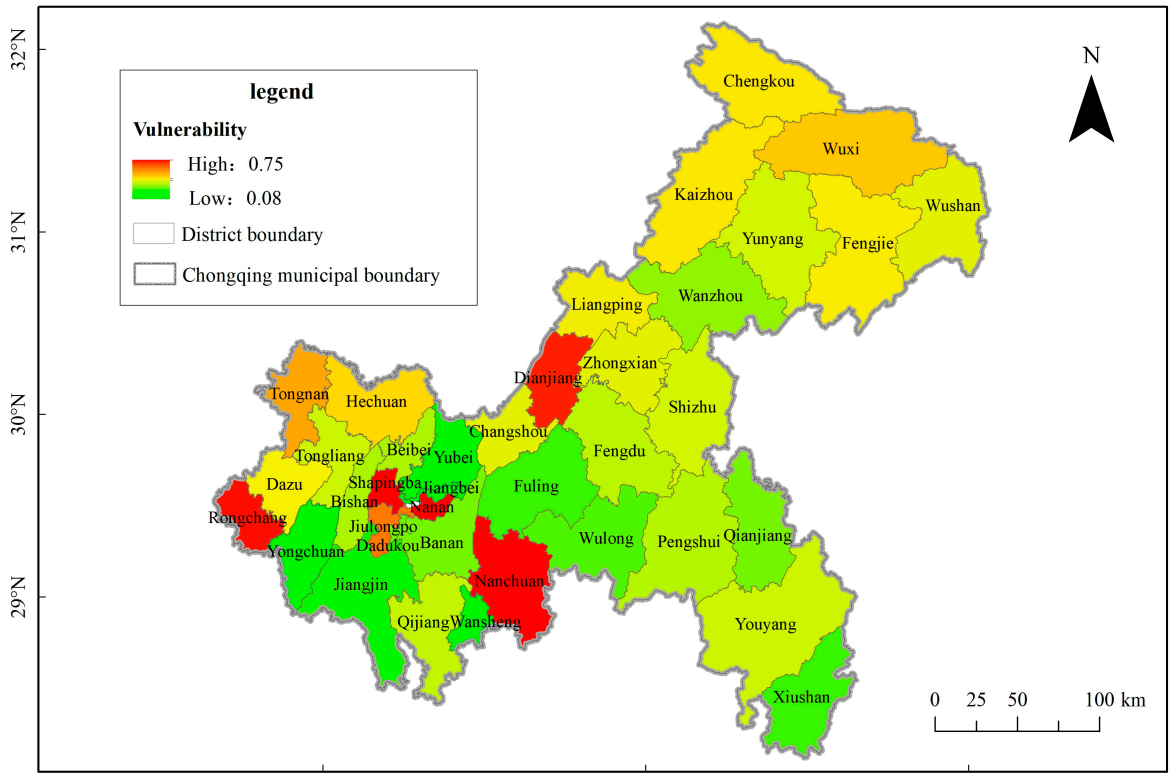


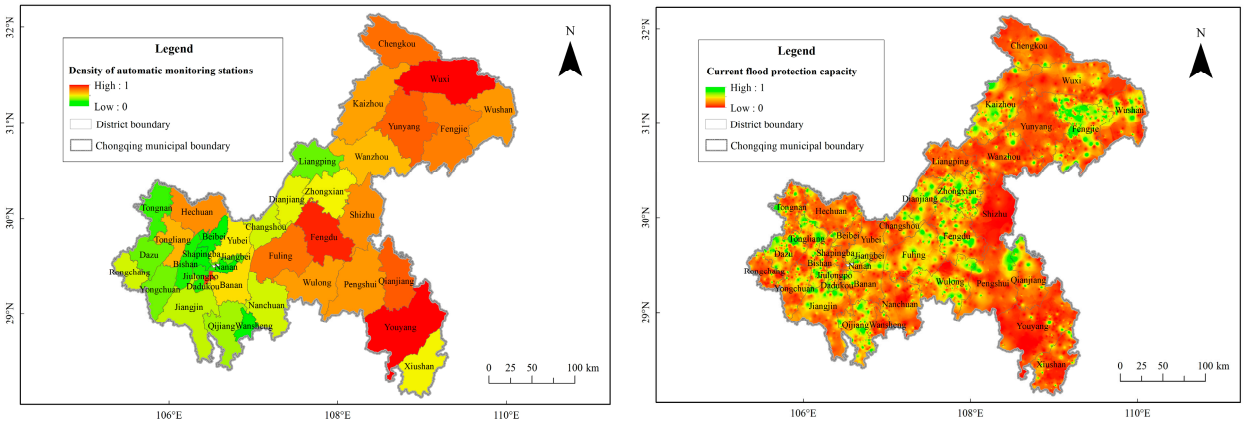
Figure 8. Distribution of vulnerability indicators in Chongqing.

4.3. Analysis of Flash Flood Disaster Resistance

4.3.1. Analysis of Second-Level Index of Disaster Resistance

1. Monitoring capacity

As described in Section 3.2.3, the area of the monitoring site was calculated (Figure 9a). As the monitoring capacity was only composed of a single element of the density of automatic monitoring stations, the distribution of the monitoring capacity was similar to that of the monitoring station control area index, which showed that in the main urban area, including districts such as Beibei, Shapingba, Jiangbei, Nan'an, and Wansheng, the control area was small, monitoring stations were dense, and disaster forecasting ability was higher than in northeastern and southeastern Chongqing. This distribution pattern arose because these areas had a concentrated population at risk of flash floods, clustered monitoring stations, and a relatively small overall area, resulting in strong regional monitoring capabilities.



(**a**) Normalised density of automatic monitoring stations. (**b**) Normalised current flood protection capacity.

Figure 9. Normalised density of automatic monitoring stations (**a**) and current flood protection capacity (**b**) for Chongqing municipality.

2. Current flood protection capacity

As outlined in Section 3.2.3, the current flood control capacity was calculated (Figure 9b). Because the second-level index flood control capacity was composed of only a single element of the current flood control capacity, the index distribution of the flood control capacity was the same as that of the current flood control capacity. The current flood control capacity index showed that in the main urban areas of Jiangbei, Jiulongpo, Qijiang, and other districts, such as Fengjie, Zhongxian, Dianjiang, and other districts in northeast Chongqing, the current flood control capacity was high.

4.3.2. Analysis of First-Level Index of Disaster Resistance

Disaster resilience indicators (Figure 10) showed that districts such as Beibei and Wansheng in western Chongqing, as well as Zhongxian and Dianjiang in northeastern Chongqing, had higher disaster resilience scores and thus stronger disaster resilience. In contrast, districts such as Wuxi and Yunyang in northeastern Chongqing, and Youyang and Fengdu in southeastern Chongqing, had lower disaster resilience scores and weaker disaster resilience. This distribution was attributed to the fact that western Chongqing was located within the main urban area, where flash flood monitoring capabilities were advanced, the economy was developed, and existing flood control infrastructure was relatively well-developed, resulting in stronger flood control capabilities.

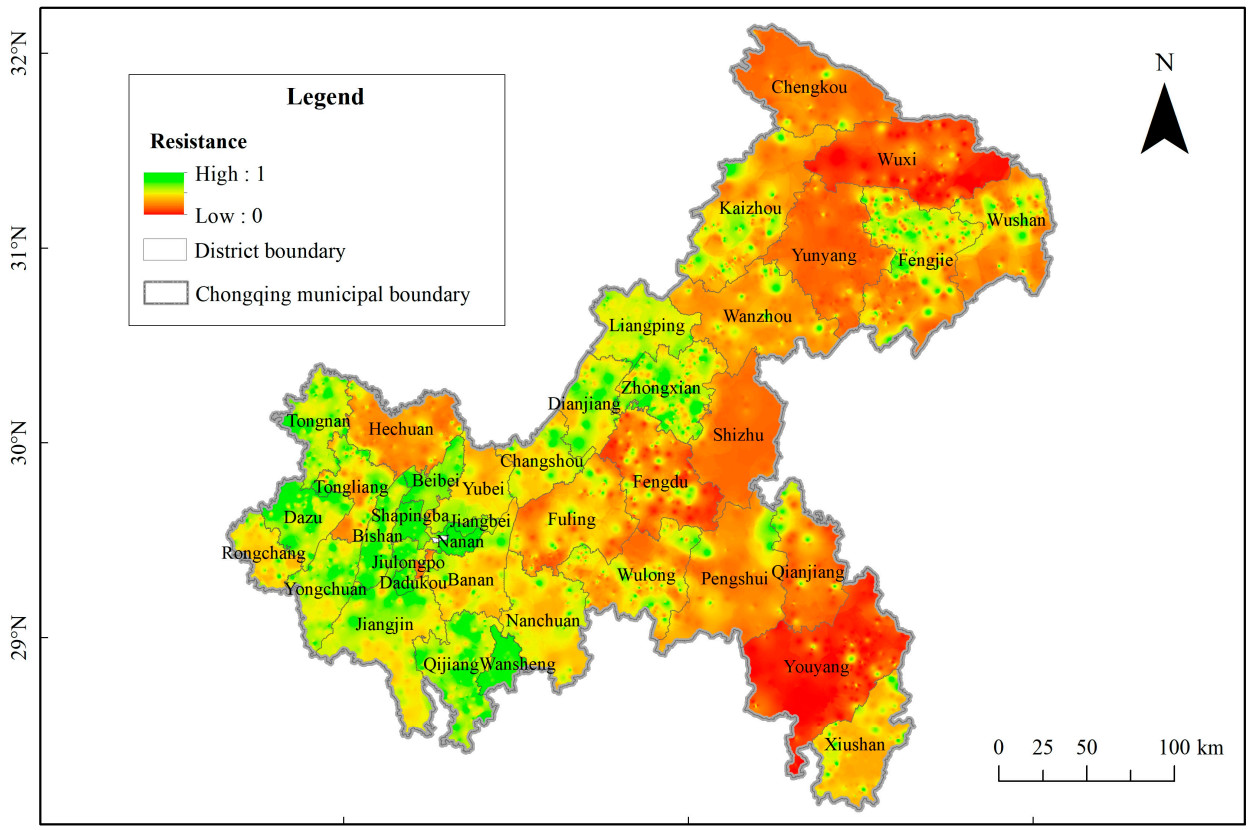


Figure 10. Distribution of resistance indicators in Chongqing.

4.4. Risk Degree of Flash Flood Disaster

Based on the risk assessment model and weights of hazard, vulnerability, and resilience indicators, the distribution of flash flood risk values in Chongqing was obtained (Figure 11). The risk value of flash flood disasters in Chongqing ranged from 0.24 to 0.69. Hechuan, Rongchang, Nan'an, Shapingba, and other districts in western Chongqing, Wuxi, Chengkou, and other districts in northeast Chongqing, Youyang, Pengshui, Shizhu, and other districts in southeastern Chongqing had larger risk values and a higher risk of flash flood disasters. Wansheng, Qijiang, Jiangjin, and other districts in western Chongqing; Fengjie, Zhongxian, Wanzhou, and other districts in northeast Chongqing, and Qianjiang, Wulong, and other districts in southeastern Chongqing, had smaller risk values and a lower risk of flash flood disasters. Overall, the risk of flash floods was higher in southeastern and northeastern Chongqing than in western Chongqing. This was mainly because these areas are located within the northwest-trending Daba Mountains' tectonic belt, which is characterised by heavy precipitation, high elevations, and steep slopes. In addition, they are economically less developed, cover large territories, and offer only limited sites where flood control investments could be effectively targeted.

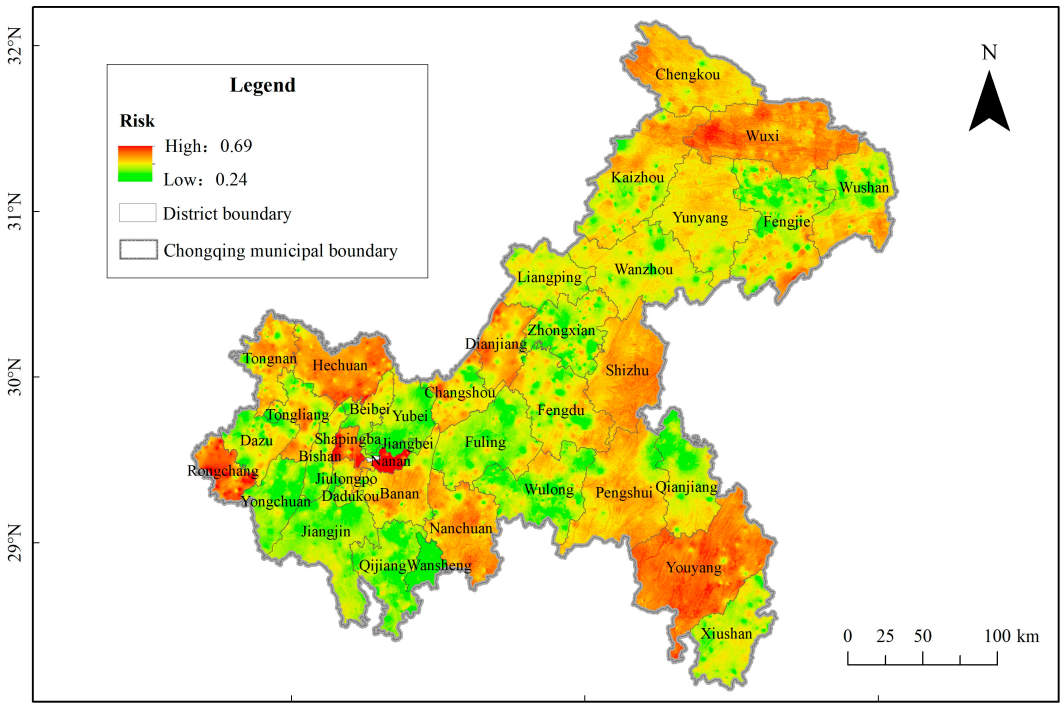


Figure 11. Flash flood disaster risk distribution map in Chongqing.

4.5. Flash Flood Disaster Risk Zone Division

According to the distribution map of the flash flood disaster risk, the Iso clustering unsupervised classification was used to grade the flash flood disaster risk. In this study, risk was divided into four levels, corresponding to low-, medium-, high-, and extremely high-risk areas (Figure 12), and the meaning of the divisions is presented in Table 12.

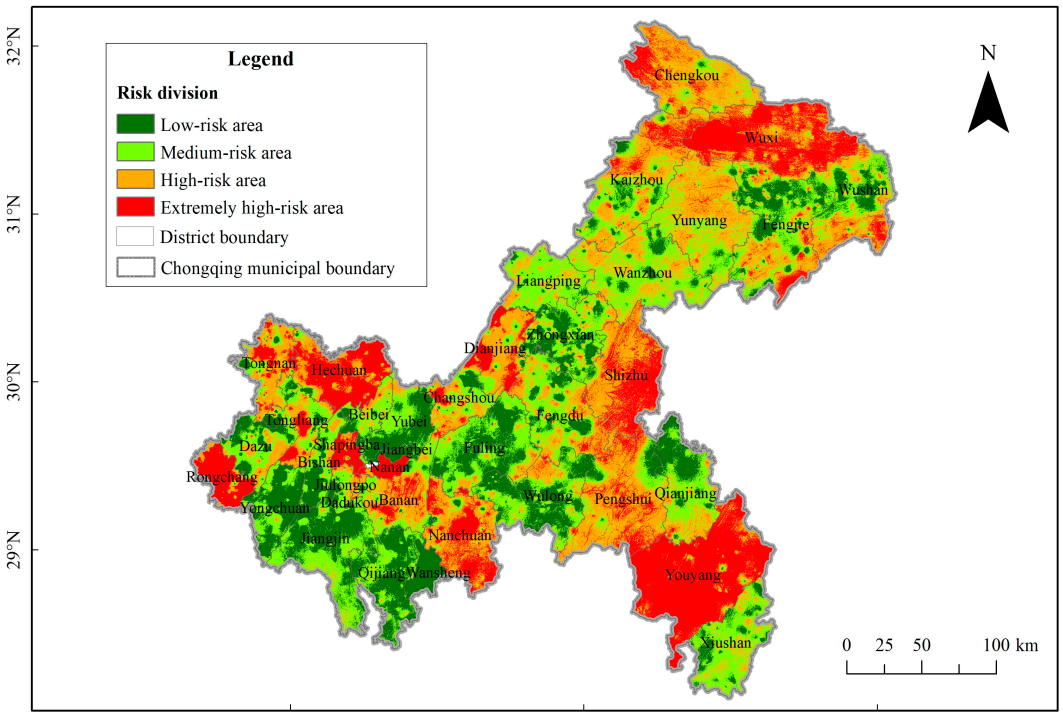


Figure 12. Chongqing flash flood disaster risk zone map.

Table 12. Flash flood disaster risk classification table.

Serial Number	Grading	Disaster Implication
1	Low-risk area	The possibility of flash floods is extremely low, causing little damage and almost no impact.
2	Medium-risk area	The possibility of a flash flood disaster is low, and the impact on personnel, farmland, and roads is small.
3	High-risk area	The possibility of a flash flood disaster is high, and it has a certain impact on mountain residents, farmland, and roads.
4	Extremely high-risk area	The possibility of a flash flood disaster is very high, as flash floods are very likely to cause casualties, farmland inundation, and housing and road damage, causing serious property losses.

Under China's mountain flood disaster prevention and control planning, all districts and counties of Chongqing Municipality, except Yuzhong District, have been designated as mountain flood disaster prevention and control areas. The total area of flash flood disaster risk in Chongqing was 82,348 km^2, and the high-risk area was 24,829 km^2, accounting for the largest proportion (30.15%). The middle-risk area was second, with an area of 24,619 km^2, accounting for 29.9%; the extremely high-risk area covered 17,559 km^2, accounting for 21.32%; and the low-risk area covered 15,342 km^2, accounting for the smallest proportion (18.63%).

This study calculated the area and proportion of each risk level across all districts and counties. From the administrative division perspective (Table 13), extremely high-risk areas were mainly concentrated in Wuxi in northeast Chongqing, Youyang and Shizhu in southeast Chongqing, and the districts of the main city, such as Nan'an, Rongchang, and Hechuan. The high-risk areas were mainly distributed in Chengkou, Yunyang, Pengshui, Tongnan, Nanchuan, Changshou, and other districts.

Table 13. Statistical Table of flash flood hazard zones in Chongqing's districts and counties.

District (County)	Low-Risk Area		Medium-Risk Area		High-Risk Area		Extremely High-Risk Area	
	Area (km^2)	Proportion	Area (km^2)	Proportion	Area (km^2)	Proportion	Area (km^2)	Proportion
Banan	77.05	4.2%	568.74	31.2%	900.15	49.4%	276.14	15.2%
Beibei	151.79	20.2%	424.13	56.5%	164.91	22.0%	9.90	1.3%
Bishan	404.85	44.2%	381.47	41.7%	127.97	14.0%	1.30	0.1%
Chengkou	27.72	0.8%	554.87	16.9%	2043.18	62.2%	661.57	20.1%
Dadukou	12.80	12.5%	23.36	22.9%	61.89	60.6%	4.02	3.9%
Dazu	482.00	33.6%	584.70	40.7%	358.96	25.0%	9.22	0.6%
Dianjiang	18.58	1.2%	215.62	14.2%	794.93	52.5%	485.81	32.1%
Fengdu	447.00	15.4%	1200.92	41.3%	1068.40	36.8%	189.39	6.5%
Fengjie	1061.97	25.9%	1509.62	36.8%	1196.66	29.2%	330.35	8.1%
Fuling	1292.69	43.9%	1355.67	46.1%	282.83	9.6%	11.93	0.4%
Hechuan	6.44	0.3%	87.69	3.7%	618.75	26.4%	1630.23	69.6%
Jiangbei	193.19	87.4%	27.72	12.5%	0.04	0.0%	0.00	0.0%
Jiangjin	1612.86	50.1%	1501.73	46.7%	102.83	3.2%	0.45	0.0%
Jiulongpo	43.50	10.0%	208.49	48.0%	141.45	32.6%	40.58	9.4%
Kaizhou	372.65	9.4%	1335.54	33.7%	1749.94	44.2%	503.87	12.7%
Liangping	130.34	6.9%	1325.69	70.1%	427.34	22.6%	6.54	0.3%
Nan'an	0.00	0.0%	0.00	0.0%	0.31	0.1%	261.22	99.9%
Nanchuan	34.11	1.3%	132.65	5.1%	1315.33	50.8%	1106.82	42.8%

Table 13. *Cont.*

District (County)	Low-Risk Area		Medium-Risk Area		High-Risk Area		Extremely High-Risk Area	
	Area (km^2)	Proportion	Area (km^2)	Proportion	Area (km^2)	Proportion	Area (km^2)	Proportion
Pengshui	232.22	6.0%	570.14	14.6%	2350.47	60.4%	741.13	19.0%
Qijiang	1350.68	62.2%	781.44	36.0%	40.83	1.9%	0.14	0.0%
Qianjiang	811.39	33.9%	1026.61	42.9%	520.55	21.8%	33.23	1.4%
Rongchang	1.99	0.2%	18.20	1.7%	146.26	13.6%	910.15	84.5%
Shapingba	0.81	0.2%	2.18	0.5%	58.83	14.8%	336.16	84.5%
Shizhu	3.49	0.1%	104.77	3.5%	1503.50	49.9%	1403.05	46.5%
Tongliang	225.65	16.8%	425.98	31.7%	465.06	34.7%	225.47	16.8%
Tongnan	86.32	5.4%	304.40	19.2%	855.86	54.0%	337.63	21.3%
Wansheng	571.40	99.6%	2.42	0.4%	0.00	0.0%	0.00	0.0%
Wanzhou	308.11	8.9%	2112.05	61.2%	1021.36	29.6%	11.79	0.3%
Wushan	571.81	19.4%	978.91	33.1%	1135.28	38.4%	268.61	9.1%
Wuxi	2.08	0.1%	73.97	1.8%	1188.67	29.6%	2755.19	68.5%
Wulong	1405.27	48.6%	1092.85	37.8%	364.43	12.6%	27.00	0.9%
Xiushan	437.72	17.9%	1640.11	66.9%	372.21	15.2%	2.14	0.1%
Yongchuan	1026.00	65.2%	525.90	33.4%	21.56	1.4%	0.00	0.0%
Youyang	3.91	0.1%	35.22	0.7%	441.63	8.5%	4686.18	90.7%
Yubei	832.40	57.1%	538.89	37.0%	85.67	5.9%	0.33	0.0%
Yunyang	85.03	2.3%	1450.61	39.9%	2013.32	55.3%	89.56	2.5%
Changshou	149.89	10.5%	497.21	35.0%	584.63	41.1%	189.96	13.4%
Zhongxian	865.91	39.7%	998.62	45.8%	302.77	13.9%	11.72	0.5%

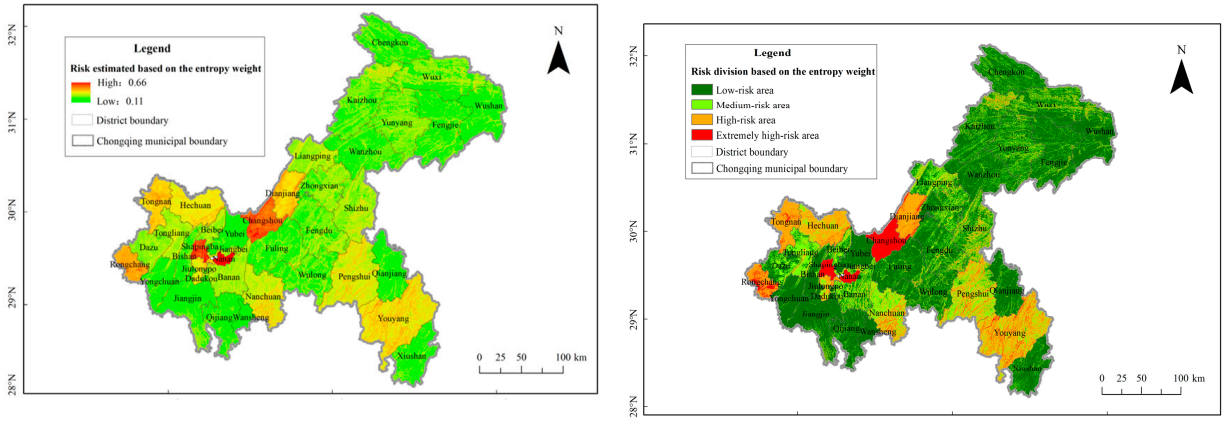
5. Discussion

The evaluation framework based on AHP is widely used in risk assessment, which views the object as a system and makes decisions based on the thinking of decomposition, comparison, judgement, and synthesis. Many researchers have used this framework to conduct risk assessments of floods, urban flooding, and other disasters [14–16,33,34]. The accuracy of mountain flood disaster risk assessment plays a very important role in the later mountain flood disaster prevention. Considering the limitations of the evaluation framework, it is necessary to verify the risk assessment results of mountain flood disasters. To verify the reliability of the AHP-based risk assessment framework, this study calculated the weight of each indicator and the flash flood risk using the entropy weighting method [19] (Table 14), an objective weighting approach. Additionally, the results obtained from the two methods were compared and validated against historical flash flood event sites.

Table 14. Indicator weights based on the entropy weighting method.

Tertiary Indicators		Entropy Weight		
Indicators	Entropy value	Tertiary indicators	Secondary indicators	Primary indicators
CE1	0.9995	0.0083	0.0107 (MC1)	0.5274 (E)
CE2	0.9998	0.0024		
CE3	0.9854	0.2210	0.5167 (UC)	
CE4	0.9936	0.0965		
CE5	0.9869	0.1992		
CV1	0.9783	0.3290	0.329 (P)	0.4042 (V)
CV2	0.9950	0.0752	0.0752 (EP)	
CR1	0.9974	0.0390	0.039 (MC2)	0.0684 (R)
CR2	0.9981	0.0294	0.0294 (FP)	

According to the flash flood risk assessment and zoning for Chongqing (Figure 13, Table 15), which was derived using the entropy weighting method, the risk values ranged from 0.11 to 0.66. The low-risk, medium-risk, high-risk, and extremely high-risk zones accounted for 53.62%, 24.95%, 17.09%, and 4.34% of the total area, respectively. It was worth noting that high-risk areas were primarily concentrated in parts of western Chongqing, which contradicted the fact that flash floods frequently occurred in the southeastern and northeastern regions of the municipality.



(**a**) Flash flood disaster risk distribution map. (**b**) Flash flood disaster risk zone map.

Figure 13. Flash flood disaster risk distribution map (**a**) and risk zone map (**b**) based on the entropy weight in Chongqing.

Table 15. Risk zoning in Chonqing using two weighting methods.

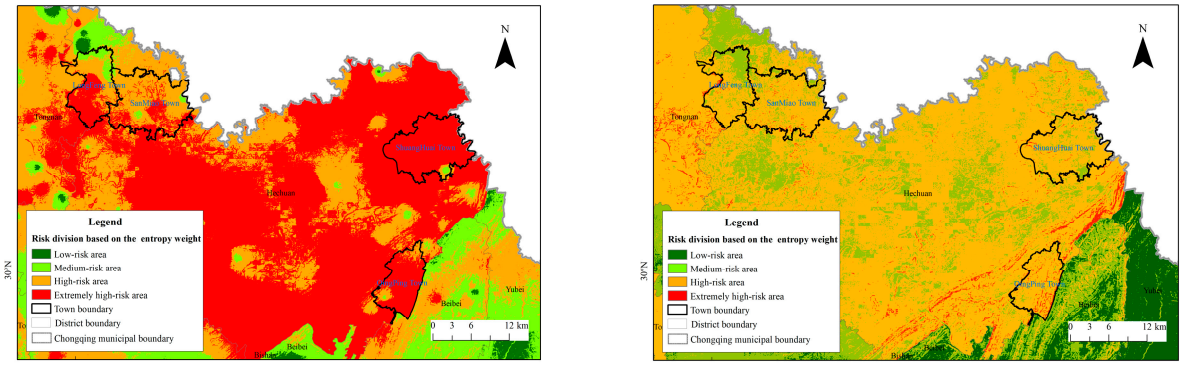
Division	AHP-Based Classification		Entropy-Based Classification	
	Area (km^2)	Proportion	Area (km^2)	Proportion
Low-risk area	15,342	18.63%	44,156	53.62%
Medium-risk area	24,619	29.90%	20,548	24.95%
High-risk area	24,829	30.15%	14,070	17.09%
Extremely high-risk area	17,559	21.32%	3575	4.34%

In this study, a total of 809 historical flash flood sites were collected. Risk zoning was based on AHP following spatial matching, and the proportions of these sites located in the low-, medium-, high-, and extremely high- risk zones were 16.56%, 27.19%, 40.17% and 16.07%, respectively (Table 16). Similarly, these locations were spatially matched with risk zones defined using the entropy-weighted method, and the proportions of these sites located in the low-, medium-, high-, and extremely high- risk zones were 57.97%, 28.55%, 9.02%, and 4.45%, respectively (Table 16). Further statistical analysis under the AHP-based classification revealed that 56.24% of the sites were located in high-risk zones and above, while 83.44% were in medium-risk zones and above. In contrast, under the entropy-based classification, 13.47% and 42.03% of the sites were located in the high-risk and medium-risk zones, respectively.

Table 16. Risk zoning of historical flash flood disaster sites using two weighting methods.

Division	AHP-Based Classification		Entropy-Based Classification	
	Number of Disaster Sites	Proportion	Number of Disaster Sites	Proportion
Low-risk area	134	16.56%	469	57.97%
Medium-risk area	220	27.19%	231	28.55%
High-risk area	325	40.17%	73	9.02%
Extremely high-risk area	130	16.07%	36	4.45%

Recognising that evaluating model performance based solely on the risk levels of specific locations may have limited validity, the study further searched for additional historical flash flood disaster records. We identified disaster data for Hechuan District, which came from the district government's flash flood disaster prevention plan (https://www.hc.gov.cn/xxgk/zfxxgkmlrk/zcwj_11903/qtwj/202406/t20240604_13264655.html (accessed on 18 May 2026)). This plan introduced the historical flash flood situations in Hechuan District and, for the period after 2017, mainly mentioned disaster impacts in Qingping Town, Shuanghuai Town, Sanmiao Town, and Longfeng Town. We compared the flash flood risk zoning of these towns, and the results showed that a higher proportion of their areas fell within high-risk or above zones in the AHP-based risk map (the area classified as high-risk or higher accounts for 95.38%; under another method, it accounts for 81.86%), further demonstrating the reliability of our research framework (Figure 14, Table 17).



(**a**) Risk zone map based on AHP.

(**b**) Risk zone map based on the entropy weight.

Figure 14. Flash flood disaster risk zone map based on AHP (**a**) and the entropy weight (**b**) in four towns.

Historically documented flash flood hazard sites are expected to be located in higher-risk zones. In this study, the flash flood risk assessment results derived from the expert scoring method and the entropy weight method were compared. The comparison showed that a higher proportion of historical flash flood sites were situated in high-risk zones in the AHP-based map, indicating better agreement with the recorded disaster locations. We further examined loss data from recent flash flood events in Hechuan District and found that the affected towns also fell predominantly within high-risk or above categories in the AHP-based zoning. These results substantiated the reliability of the AHP-based framework in identifying flash-flood-prone areas. Further analysis of the entropy weight method revealed that, because it relied solely on intrinsic data information, certain indicators that strongly influence flash flood risk (e.g., design rainstorm and threshold rainfall) received relatively low weights. As a result, the entropy-based risk distribution tended to assign low

risk to areas that were actually prone to flash floods, highlighting the limitations of a purely data-driven weighting approach in this context. Nevertheless, this research framework was better suited to regions where flash flood disaster survey and evaluation data were available, although it did not incorporate physical processes into the risk assessment. Future work could integrate hydrological and hydrodynamic models to enhance the objectivity of risk classification.

Table 17. Risk zoning in four towns using two weighting methods.

Method	Town	Low-Risk Area		Medium-Risk Area		High-Risk Area		Extremely High-Risk Area	
		Area (km^2)	Proportion	Area (km^2)	Proportion	Area (km^2)	Proportion	Area (km^2)	Proportion
AHP-based	LongFeng	0.1116	0.2%	10.2177	15.4%	25.8867	39.0%	30.1167	45.4%
	QingPing	0	0.0%	1.0917	1.2%	2.4318	2.6%	91.3383	96.3%
	SanMiao	0	0.0%	3.042	3.0%	68.1777	67.4%	29.871	29.5%
	ShuangHuai	0	0.0%	0.3195	0.6%	8.7903	15.3%	48.3066	84.1%
	Sum	0.1116	0.0%	14.6709	4.6%	105.2865	32.9%	199.6326	62.4%
Entropy-based	LongFeng	0	0.0%	23.7672	35.8%	42.0822	63.4%	0.4833	0.7%
	QingPing	0	0.0%	14.526	15.3%	79.2603	83.6%	1.0755	1.1%
	SanMiao	0	0.0%	16.8894	16.7%	81.945	81.1%	2.2563	2.2%
	ShuangHuai	0.0108	0.0%	2.7909	4.9%	49.7061	86.6%	4.9086	8.5%
	Sum	0.0108	0.0%	57.9735	18.1%	252.9936	79.1%	8.7237	2.7%

6. Conclusions

In this study, we integrated multiple parameters, including rainfall and underlying surface conditions, to establish a flash flood disaster risk assessment model. This model was employed to evaluate flash flood hazard, vulnerability, disaster resilience, and overall risk, and to identify the distribution of areas of flash flood with extremely high, high, medium, and low risk in Chongqing. Additionally, we conducted a comparative analysis using an objective weighting method to validate the validity and applicability of the proposed approach.

The risk value for flash flood disasters in Chongqing ranged between 0.24 and 0.69. The risk values of Hechuan and other districts in western Chongqing, Wuxi and other districts in northeastern Chongqing, and Youyang and other districts in southeastern Chongqing were large, and the risk of flash flood disasters was high. Wansheng, and other districts in western Chongqing, Fengjie, and other districts in northeast Chongqing, and Qianjiang, and other districts in southeastern Chongqing, had smaller risk values and a lower risk of flash flood disasters.

In the risk zones of flash flood disasters in Chongqing, high-risk areas accounted for the largest proportion (30.15%), followed by medium-risk (29.90%), extremely high-risk (21.32%), and low-risk areas accounting for the least (18.63%). The extremely high-risk areas were mainly concentrated in Wuxi in northeastern Chongqing, Youyang in southeastern Chongqing, and Nan'an, Rongchang, Hechuan, and other districts in western Chongqing. High-risk areas were mainly distributed in Chengkou in northeastern Chongqing, Pengshui, and Shizhu in southeastern Chongqing, and Jiangbei and Tongnan in western Chongqing.

Author Contributions: Conceptualization, methodology, formal analysis, writing—review and editing, J.Q. and L.W.; validation and original draft preparation, L.Z. and J.N.; investigation and data curation, M.Z., Y.Y., R.Y. and W.N. All authors have read and agreed to the published version of the manuscript.

Funding: This study was jointly funded by the Science and Technology Achievement Transformation Fund, China Institute of Water Resources and Hydropower Research, grant number ZS1003A012021,

the Science and Technology Program, China Institute of Water Resources and Hydropower Research, grant number ZS0163B012021, and the National Key Research and Development Program of China, grant number 2023YFD2300304.

Institutional Review Board Statement: Not applicable.

Informed Consent Statement: Not applicable.

Data Availability Statement: The datasets generated and analysed during the current study are not publicly available, but they are available from the corresponding author on reasonable request.

Conflicts of Interest: The authors declare no conflicts of interest. Ms. Jie Niu is an employee of Jinan Water Conservancy Building Survey, Design and Research Institute Co., Ltd. The paper reflects the views of the scientists and not the company.

Abbreviations

The following abbreviations are used in this manuscript:

AHP	Analytic hierarchy process
DEM	Digital elevation model
NDVI	Normalised Difference Vegetation Index
GDP	Gross domestic product
FA	Factor analysis
KMO	Kaiser–Meyer–Olkin

References

1. Ma, M.; Zhao, G.; He, B.; Li, Q.; Dong, H.; Wang, S.; Wang, Z. XGBoost-Based Method for Flash Flood Risk Assessment. *J. Hydrol.* **2021**, *598*, 126382. [CrossRef]
2. He, B.S.; Ma, M.H.; Li, Q.; Liu, L.; Wang, X.H. Current Situation and Characteristics of Flash Flood Prevention in China. *China Rural Water Hydropower* **2021**, 133–138+144. Available online: https://irrigate.whu.edu.cn/CN/Y2021/V0/I5/133 (accessed on 18 May 2026).
3. Tan, L.; Schultz, D.M. Damage Classification and Recovery Analysis of the Chongqing, China, Floods of August 2020 Based on Social-Media Data. *J. Clean. Prod.* **2021**, *313*, 127882. [CrossRef]
4. Song, G.Y.; Yan, T.J.; Xie, Q.; Lu, Y. Construction and Effect of Flash Flood Disasters Prevention System in Chongqing. *China Flood Drought Manag.* **2020**, *30*, 127–129.
5. IPCC. *IPCC Climate Change 2021: The Physical Science Basis*; IPCC: Geneva, Switzerland, 2021.
6. Zhou, B.T.; Qian, J. Changes of Weather and Climate Extremes in the IPCC AR6. *Adv. Clim. Change Res.* **2021**, *17*, 713–718.
7. Wang, L.; Huang, S.; Huang, Q.; Leng, G.; Han, Z.; Zhao, J.; Guo, Y. Vegetation Vulnerability and Resistance to Hydrometeorological Stresses in Water- and Energy-Limited Watersheds Based on a Bayesian Framework. *Catena* **2021**, *196*, 104879. [CrossRef]
8. Yildirim, E.; Just, C.; Demir, I. Flood Risk Assessment and Quantification at the Community and Property Level in the State of Iowa. *Int. J. Disaster Risk Reduct.* **2022**, *77*, 103106. [CrossRef]
9. Zarghami, S.A.; Dumrak, J. A System Dynamics Model for Social Vulnerability to Natural Disasters: Disaster Risk Assessment of an Australian City. *Int. J. Disaster Risk Reduct.* **2021**, *60*, 102258. [CrossRef]
10. Li, W.; Lin, K.; Zhao, T.; Lan, T.; Chen, X.; Du, H.; Chen, H. Risk Assessment and Sensitivity Analysis of Flash Floods in Ungauged Basins Using Coupled Hydrologic and Hydrodynamic Models. *J. Hydrol.* **2019**, *572*, 108–120. [CrossRef]
11. Lin, K.; Chen, H.; Xu, C.-Y.; Yan, P.; Lan, T.; Liu, Z.; Dong, C. Assessment of Flash Flood Risk Based on Improved Analytic Hierarchy Process Method and Integrated Maximum Likelihood Clustering Algorithm. *J. Hydrol.* **2020**, *584*, 124696. [CrossRef]
12. Wu, Z.; Bhattacharya, B.; Xie, P.; Zevenbergen, C. Improving Flash Flood Forecasting Using a Frequentist Approach to Identify Rainfall Thresholds for Flash Flood Occurrence. *Stoch. Environ. Res. Risk Assess.* **2023**, *37*, 429–440. [CrossRef]
13. Sahrane, R.; Bounab, A.; El Kharim, Y.; Obda, O.; El Miloudi, Y.; Mihraje, A.; Ahniche, M.; El Afi, M. Landslide–Anthropogenic Interactions in Urban Areas: A Multidisciplinary Case Study from Taounate. *Geotech. Geol. Eng.* **2025**, *43*, 238. [CrossRef]
14. Kumar, S.; Parida, B.R.; Ahammed, K.K.B. Flood Risk Assessment of the Kosi River Basin in North Bihar Using Synthetic Aperture Radar (SAR) Data and AHP Approach. *Nat. Hazards Res.* **2025**, *5*, 618–632. [CrossRef]
15. Zhao, Y.J.; Wang, H.; Liu, Z.L.; Wu, S.; Ma, Q.Q. Multi-Scenario Waterlogging Disaster Risk Assessment Based on Combination Weighting. *Water Resour. Hydropower Eng.* **2025**, *53*, 1–12.

16. Wang, J.H.; Zhang, D.H.; Wang, Y.Y. Research and Application of Combined Empowerment Method for Urban Flood Risk: Take Huai'an City as an Example. *Water Resour. Hydropower Eng.* **2025**, *56*, 91–104. [CrossRef]
17. Nakhaei, M.; Nakhaei, P.; Gheibi, M.; Chahkandi, B.; Wacławek, S.; Behzadian, K.; Chen, A.S.; Campos, L.C. Enhancing Community Resilience in Arid Regions: A Smart Framework for Flash Flood Risk Assessment. *Ecol. Indic.* **2023**, *153*, 110457. [CrossRef]
18. Burayu, D.G.; Karuppannan, S.; Shuniye, G. Identifying Flood Vulnerable and Risk Areas Using the Integration of Analytical Hierarchy Process (AHP), GIS, and Remote Sensing: A Case Study of Southern Oromia Region. *Urban. Clim.* **2023**, *51*, 101640. [CrossRef]
19. Wu, J.; Chen, X.; Lu, J. Assessment of Long and Short-Term Flood Risk Using the Multi-Criteria Analysis Model with the AHP-Entropy Method in Poyang Lake Basin. *Int. J. Disaster Risk Reduct.* **2022**, *75*, 102968. [CrossRef]
20. Ma, Q.; Li, Q.; Hao, S.J.; Wang, X.M.; Wang, Y.Z.Y.; Gourbesville, P. Review and Analysis of "7·20" Flash Flood and Debris Flow Disaster in Hanyuan, Sichuan. *Water Resour. Hydropower Eng.* **2025**, *56*, 204–215. [CrossRef]
21. Riaz, R.; Mohiuddin, M. Application of GIS-Based Multi-Criteria Decision Analysis of Hydro-Geomorphological Factors for Flash Flood Susceptibility Mapping in Bangladesh. *Water Cycle* **2025**, *6*, 13–27. [CrossRef]
22. Luo, L.; Wang, Y.; Li, Q.; Li, M.; Wang, J.; Zhao, G.; Ma, M. Exploration of the Spatiotemporal Characteristics and Triggering Factors of Flash Flood in China. *Ecol. Indic.* **2025**, *176*, 113698. [CrossRef]
23. Hossain, M.T.; Haq, K.M.F. Flash Flood Risk Delineation Using Multi-Criteria Decision-Making (MCDM) Approach in Sylhet Basin Region, Bangladesh. *Total Environ. Adv.* **2026**, *17*, 200144. [CrossRef]
24. He, X.; Fang, Y.; Huang, X.; Yang, L.E.; Xu, Y.; Liu, J.; Guo, Y.; Zhu, A. Flash Flood Risk Governance System in China and Its Governance Effectiveness. *Environ. Impact Assess. Rev.* **2026**, *119*, 108345. [CrossRef]
25. Taghipoorreyneh, M. Mixed Methods and the Delphi Method. In *International Encyclopedia of Education*, 4th ed.; Tierney, R.J., Rizvi, F., Ercikan, K., Eds.; Elsevier: Oxford, UK, 2023; pp. 608–614.
26. Crespi, A.; Renner, K.; Zebisch, M.; Schauser, I.; Leps, N.; Walter, A. Analysing Spatial Patterns of Climate Change: Climate Clusters, Hotspots and Analogues to Support Climate Risk Assessment and Communication in Germany. *Clim. Serv.* **2023**, *30*, 100373. [CrossRef]
27. He, Y. Research on the Regulatory Effect of Chongqing Mountainous Terrain on the Thermal Environment of Courtyard Buildings: A Case Study of Huayan Temple. Master's Thesis, Chongqing University, Chongqing, China, 2024. [CrossRef]
28. Shi, X.L.; Zhang, Y.; Ding, H. Advances in natural disaster risk assessment. *J. Xi'an Univ. Technol.* **2024**, *40*, 362–372. [CrossRef]
29. Panagiotou, C.F. Copula-Based Assessment of Flood Susceptibility in the Island of Cyprus via Stochastic Multicriteria Decision Analysis. *Sci. Total Environ.* **2025**, *979*, 179469. [CrossRef]
30. Xue, W.; Wu, Z.; Xu, H.; Wang, H.; Liang, Q.; Ma, C.; Zhou, Y.; Xu, S. Comprehensive Risk Assessment of Urban Flood Process Based on Dynamic Weights and Lumped Impact Parameters. *J. Hydrol.* **2025**, *662*, 133903. [CrossRef]
31. Katarina, L.; Mirjana, T.; Tijana, V.; Siniša, P.; Natalija, M.; Milica, C. Determination of Flash Flood Hazard Areas in the Likodra Watershed. *Water* **2023**, *15*, 2698. [CrossRef]
32. Saaty, T.L.; Tran, L.T. On the Invalidity of Fuzzifying Numerical Judgments in the Analytic Hierarchy Process. *Math. Comput. Model.* **2007**, *46*, 962–975. [CrossRef]
33. Yuan, Y.; Jin, Z.W.; Zeng, X.; Jiang, X.; Guo, C. Study of Assessment of Mountain Flood Risk in Sichuan Province Considering Sediment Factor. *Express Water Resour. Hydropower* **2024**, *45*, 16–22. [CrossRef]
34. Singha, C.; Sahoo, S.; Mahtaj, A.B.; Moghimi, A.; Welzel, M.; Govind, A. Advancing Flood Risk Assessment: Multitemporal SAR-Based Flood Inventory Generation Using Transfer Learning and Hybrid Fuzzy-AHP-Machine Learning for Flood Susceptibility Mapping in the Mahananda River Basin. *J. Environ. Manag.* **2025**, *380*, 124972. [CrossRef]

Disclaimer/Publisher's Note: The statements, opinions and data contained in all publications are solely those of the individual author(s) and contributor(s) and not of MDPI and/or the editor(s). MDPI and/or the editor(s) disclaim responsibility for any injury to people or property resulting from any ideas, methods, instructions or products referred to in the content.